International Journal of Nanomedicine

Dovepress
open access to scientific and medical research

Open Access Full Text Article

ORIGINAL RESEARCH

Multilayered composite coatings of titanium dioxide nanotubes decorated with zinc oxide and hydroxyapatite nanoparticles: controlled release of Zn and antimicrobial properties against *Staphylococcus aureus*

This article was published in the following Dove Press journal:
International Journal of Nanomedicine

Urvashi F Gunputh[1,2]
Huirong Le[1]
Alexandros Besinis[2]
Christopher Tredwin[3]
Richard D Handy[4]

[1]School of Mechanical Engineering and Built Environment, University of Derby, Derby DE22 3AW, UK; [2]School of Engineering, Plymouth University, Plymouth PL4 8AA, UK; [3]Peninsula Schools of Medicine and Dentistry, Plymouth University, Plymouth, Devon PL6 8BU, UK; [4]School of Biological & Marine Sciences, Plymouth University, Plymouth PL4 8AA, UK

Purpose: This study aimed to decorate the surface of TiO_2 nanotubes (TiO_2 NTs) grown on medical grade Ti-6Al-4V alloy with an antimicrobial layer of nano zinc oxide particles (nZnO) and then determine if the antimicrobial properties were maintained with a final layer of nano-hydroxyapatite (HA) on the composite.

Methods: The additions of nZnO were attempted at three different annealing temperatures: 350, 450 and 550 °C. Of these temperatures, 350°C provided the most uniform and nanoporous coating and was selected for antimicrobial testing.

Results: The LIVE/DEAD assay showed that $ZnCl_2$ and nZnO alone were >90% biocidal to the attached bacteria, and nZnO as a coating on the nanotubes resulted in around 70% biocidal activity. The lactate production assay agreed with the LIVE/DEAD assay. The concentrations of lactate produced by the attached bacteria on the surface of nZnO-coated TiO_2 NTs and ZnO/HA-coated TiO_2 NTs were 0.13±0.03 mM and 0.37±0.1 mM, respectively, which was significantly lower than that produced by the bacteria on TiO_2 NTs alone, 1.09±0.30 mM (Kruskal–Wallis, $P<0.05$, n=6). These biochemical measurements were correlated with electron micrographs of cell morphology and cell coverage on the coatings.

Conclusion: nZnO on TiO_2 NTs was a stable and antimicrobial coating, and most of the biocidal properties remained in the presence of nano-HA on the coating.

Keywords: zinc oxide nanoparticles, TiO_2 nanotubes, hydroxyapatite, antimicrobial, Staphylococcus aureus

Introduction

Medical implants used in orthopedics or dentistry should be sufficiently durable with mechanical properties that mimic the intended tissue.[1] They must also be safe for the patients in the long term and ideally show some antimicrobial properties to minimize the infection risk right after surgery. Unfortunately, there is no single material with all these desirable properties, and in recent years attention has turned toward enhancing the properties of implants with coatings of nanomaterials.[2,3] In orthopedic and dental implants, several types of nanocomposite coatings are employed including diamond-like carbon coatings on Co/Cr alloy,[4] nanocollagen and calcium phosphate,[5] hydroxyapatite (HA) nanoparticles and polycaprolactone,[6]

Correspondence: Huirong Le
School of Mechanical Engineering and Built Environment, University of Derby, Markeaton Street, Derby DE22 3AW, UK
Email H.Le@derby.ac.uk

Richard D Handy
School of Biological & Marine Sciences, Plymouth University, Plymouth PL4 8AA, UK
Email R.Handy@plymouth.ac.uk

submit your manuscript | www.dovepress.com
DovePress
http://doi.org/10.2147/IJN.S199219

and carbon nanotubes (CNTs) reinforced with HA.[7] The purpose of such coatings has been mainly to improve biocompatibility and/or strengthen the respective implant material, rather than address antimicrobial properties.

Titanium dioxide nanotubes (TiO_2 NTs) have shown promise in such fields in the past. The nanotubes are readily grown on medical grade titanium, and they can resist mechanical stresses similar to those faced by bone.[8] They have also been shown to be biocompatible with bone cells, partly because they mimic the surface morphology of bone.[9] However, TiO_2 NTs alone are not antimicrobial, and the development of infection around bone implants is a clinical concern. Indeed, the failure of two-thirds of implants postsurgery is attributed to infection.[10] *Staphylococcus aureus* is one of the most common causes of infection in both polymer[11-13] and metallic implants.[14] To enhance antimicrobial properties of titanium implants, attempts have been made to coat TiO_2 NTs with antibiotics such as gentamicin[15] or vancomycin.[16] However, infections related to implants are normally caused by a consortium of microbes.[17] Individual antibiotics are inevitably only targeting at a few of the organisms present. There is also the concern that antibiotic resistance can develop during the treatment.[18] Alternatively, dissolved metallic elements such as silver, copper, and zinc have been known for their antimicrobial properties for centuries. Their solubility and biological reactivity have restricted their applications to simple disinfectants in the past, but now nanoparticulate forms of these metals are available. Of these metals, silver nanoparticles are arguably the strongest biocide with minimum inhibitory concentrations (MICs) of 3.25 mg/L to *Streptcoccus mutans*[19] and silver nanoparticles are also toxic to *S. aureus* when silver is presented as a filler in chitosan[20,21] or a coating on medical grade titanium alloy.[22]

However, from a clinical safety perspective, silver remains a nonessential toxic element that should not normally be present in the human body. It is, therefore, more desirable to use a nutritionally required metal, such as zinc, that is easily handled and excreted by the human body, but at the same time antimicrobial. Zinc oxide nanoparticles (nZnO) have antibacterial properties against both Gram-positive and Gram-negative bacteria. For example, nZnO was found to be an effective bactericide against *Escherichia coli*, as measured by Varaprasad et al.[23] In the latter study, the inhibition zone for the nano-zinc oxide containing fibers was between 2.1 and 3.6 mm in an agar diffusion plate test. A minimum of 100 μg/mL of nZnO in suspension was found to be antibacterial against both Gram-positive bacteria (*S. mutans and S. pyogenes*) and Gram-negative bacteria (*Vibrio cholerae, Shigella flexneri,* and *Salmonella typhii*) as measured by MIC assay after 12 hrs exposure in Muller–Hinton broth.[24] The effect of particle shape and size on toxicity is still being debated.[25] Apparently, it is the method of synthesis that determines the initial shape, size and morphology of zinc-containing nanoparticles.[26]

There are several techniques for growing nZnO on the surface of TiO_2 NTs. These include a hydrothermal method, electrodeposition, pyrolysis deposition, atomic layer deposition, self-assembled monolayers, and others.[27,28] These methods give rise to nZnO of different shapes and dimensions, such as flower-like, hexagonal rod-like and spherical-like particles.[26] All of the various shapes have been shown to have antibacterial properties, with the smallest sizes generally exhibiting the highest antibacterial properties.[25] However, the challenge is to firmly attach the nZnO to the surface of the TiO_2 NTs such that the integrity of the composite is not compromised and so that the antimicrobial activity persists. In some cases, nZnO particles are formed with uneven coverage on the surface of the nanotubes.[29,30] Other researchers were able to get uniformly distributed nZnO particles on the surface of TiO_2 NTs.[31,32] Annealing can also affect the size of the nZnO particles on the nanotubes;[32] and higher annealing temperature tends to give improved stoichiometry of nZnO relative to other components in the composite.[33]

The biocompatibility of the external surface of the composite also needs to be considered in the context of the fibroblasts involved in wound healing and the osteoblasts that are critical to the osseointegration of the implant into the surrounding bone. There is evidence that nZnO can also have some toxicity to mammalian cells (epithelial cells),[34,35] and so it may be desirable to moderate any direct contact of the nZnO with the human tissue. HA is a bioceramic material which has a similar structure to bone and is well known as a biocompatible material that promotes osseointegration.[7,36] Nanoforms of HA are also available in this regard.[37] This study aimed to develop a process to decorate TiO_2 NTs grown on Ti-6Al-4V alloy discs with a uniform coating of nZnO. The synthesis of the nZnO coating was optimized by exploring different annealing temperatures. The composite coating was then made with a nano-HA top coat. To demonstrate the antimicrobial properties, the resulting composite coatings were tested against *S. aureus*. This microbe is

considered to be one of the main causes of infection in orthopedic implants[38] and was hence used for testing the biocidal properties of the nZnO coatings. For these latter studies, the approaches included counting the proportions of live and dead bacteria on the coatings, monitoring microbial activity with a lactate production assay, as well as electron microscopy to observe coating integrity and the presence of any bacteria.

Materials and method

The material fabrication process involved the synthesis of TiO_2 NTs by anodizing the surface of medical grade titanium alloy that was subsequently doped with nZnO to incorporate some antibacterial properties. The nZnO was allowed to incorporate as crystal growing on the surface of the TiO_2 NTs. Then, a final HA mineral was added to form a composite coating. The composite coatings were characterized and then tested for their antibacterial properties against *S. aureus*.

Growth of TiO_2 NTs with nZnO and HA coating

A sheet of medical grade Ti-6Al-4V alloy of 1 mm thickness (William Gregor Ltd, London, UK) was initially laser cut into 15 mm discs (Laser Industries Ltd, Saltash, UK). The alloy was then polished with #400, #800, and #1,200 grit silicon carbide paper (Elektron Technology Ltd, Torquay, UK). Subsequently, the discs were further polished with 6 micron and 1 micron diamond paste (Agar Scientific, Stansted, UK), after which they were cleaned by ultrasonication (12 MHz) in a mixture of NaOH (1 mol/L), $NaHCO_3$ (1 mol/L) and Na $C_6H_7O_7$ (1.5 mol/L) in a ratio of 1: 1: 1.5, respectively, for 10 mins. The TiO_2 NTs were then grown on the cleaned surface of the Ti-6Al-4V alloy and then characterized following the optimized protocol described in the previous paper.[39] Briefly, TiO_2 NTs of an external diameter of 116.2 ±6.4 nm (mean ± SEM, n=54) were grown on the surface of the Ti-6Al-4V alloy by anodizing. This involved immersing the alloy for 1 hr in a mixture of 1 mol/L NH_4HPO_4 and 5 g/L NH_4F (0.5 g of NH_4F in 100 mL of ammonia solution). The solution was adjusted to pH 4 with 1 mol/L phosphoric acid. The samples were anodized at a voltage of 20 V, with an initial sweep rate of 0.5 V/s, using a dual-output programmable power supply (Metrix Electronics Limited, Tadley, UK). The Ti-6Al-4V discs with the freshly grown TiO_2 NTs were then annealed at 350 ºC for 2 hrs in a furnace (Carbolite RWF 1200, Carbolite Engineering Services, Hope Valley, UK). Care was taken to provide a gradual increase in temperature and gradual decrease back to room temperature during the annealing to ensure the final crystalline phase of the nanotubes was anatase.[40] Afterward, the TiO_2 NTs were functionalized with –OH groups by treating them with 2 mol/L NaOH at 50°C for 2 mins.[41] This provided a reactive surface for the next steps in the synthesis of the composite material.

A modified version of the protocol by Liu et al[42] was used for the synthesis of nZnO on the TiO_2 NTs. In order to determine the appropriate concentration of chemicals required to grow nZnO, pilot trials were performed (Figure S1), cumulating in the following procedure. The Ti-6Al-4V discs with the functionalized TiO_2 NTs were immersed in a 1:2 mixture of 0.075 mol/L analytical grade $Zn(NO_3)_2$ (prepared in ultrapure deionized water) and 0.1 mol/L hexamethylenetetramine (prepared in dilute ammonia), with 2 mg analytical grade citric acid. The mixture was subsequently heated to 80ºC, with continuous stirring on a magnetic hot plate. After 2 hrs in the mixture, the alloy discs of TiO_2 NTs now with the nZnO present were sonicated in deionized water for 10 mins to wash the coatings and remove any loosely bound materials and dissolved zinc.

The next step involved stabilizing the crystalline structure of the nZnO onto the TiO_2 NTs (hereafter, called TiO_2–ZnO). Little is known about the formation of nZnO crystals on the surface of novel structures such as TiO_2 NTs, and so this step was performed at three different annealing temperatures (350, 450, and 550ºC) in order to explore the resulting material morphology, surface roughness, and chemical composition. The annealing was performed in triplicate, by gradual heating of the samples to the required temperature in a furnace (Carbolite RWF 1200). The samples were maintained at the desired final temperature for 1 hr, before being allowed to gradually cool to room temperature. The resulting coatings are hereafter termed as TiO_2–ZnO/350, TiO_2–ZnO/450, and TiO_2–ZnO/550 in relation to the annealing temperatures of 350, 450, and 550ºC, respectively. A control for the annealing treatment was the unheated TiO_2–ZnO discs for comparison. The resulting discs were examined for morphology and elemental composition of the surfaces (in triplicate) by scanning electron microscopy (JEOL7001F SEM) coupled with energy-dispersive X-ray spectroscopy (EDS). The EDS composition was described using the AZtec analysis software supplied with the EDS attachment (Oxford Instruments, Oxford, UK). In addition, surface roughness

was measured using an Olympus Laser Microscope LEXT OLS3100. The characterization of all of the TiO_2–ZnO composites at the end of this step of the synthesis is shown in Figure 1.

The final step in the overall synthesis of the composite coating was to add HA. Each of the nZnO-coated materials from the step above (from all annealing temperatures) was separately immersed in 3 times the normal concentration of a simulated body fluid (3SBF) which was prepared using a concentrated version of Kokubo's recipe (in mmol/L): Na^+426, K^+15.0, Mg^{2+}4.5, Ca^{2+}7.5, Cl^- 443.4, HCO_3^- 12.6, HPO_4^{2-} 3.0, and SO_4^{2-} 1.5 mmol/L.[43] To make 1 L of this concentrated SBF in ultrapure water, the following salts were added: 7.996 g NaCl, 0.350 g $NaHCO_3$, 0.224 g KCl, 0.228 g $K_2HPO_4.3H_2O$, 0.305 g $MgCl_2.6H_2O$, 0.278 g $CaCl_2$, 0.071 g Na_2SO_4, 6.057 g $(CH_2OH)_3CNH_2$, and 40 mL of 1 mol/L HCl. Fine adjustments were made with the same dilute HCl to achieve a final pH value of 7.4. The exposure was maintained at 37ºC for 24 hrs with the aim of growing HA crystals on the surface of the samples.[43] After 24 hrs, the resulting HA-coated composites were removed, washed in deionized water, then air-dried, and examined by electron microscopy for morphology and for surface roughness as above. The 3SBF media (n=15 in total) were retained for metal analysis to determine

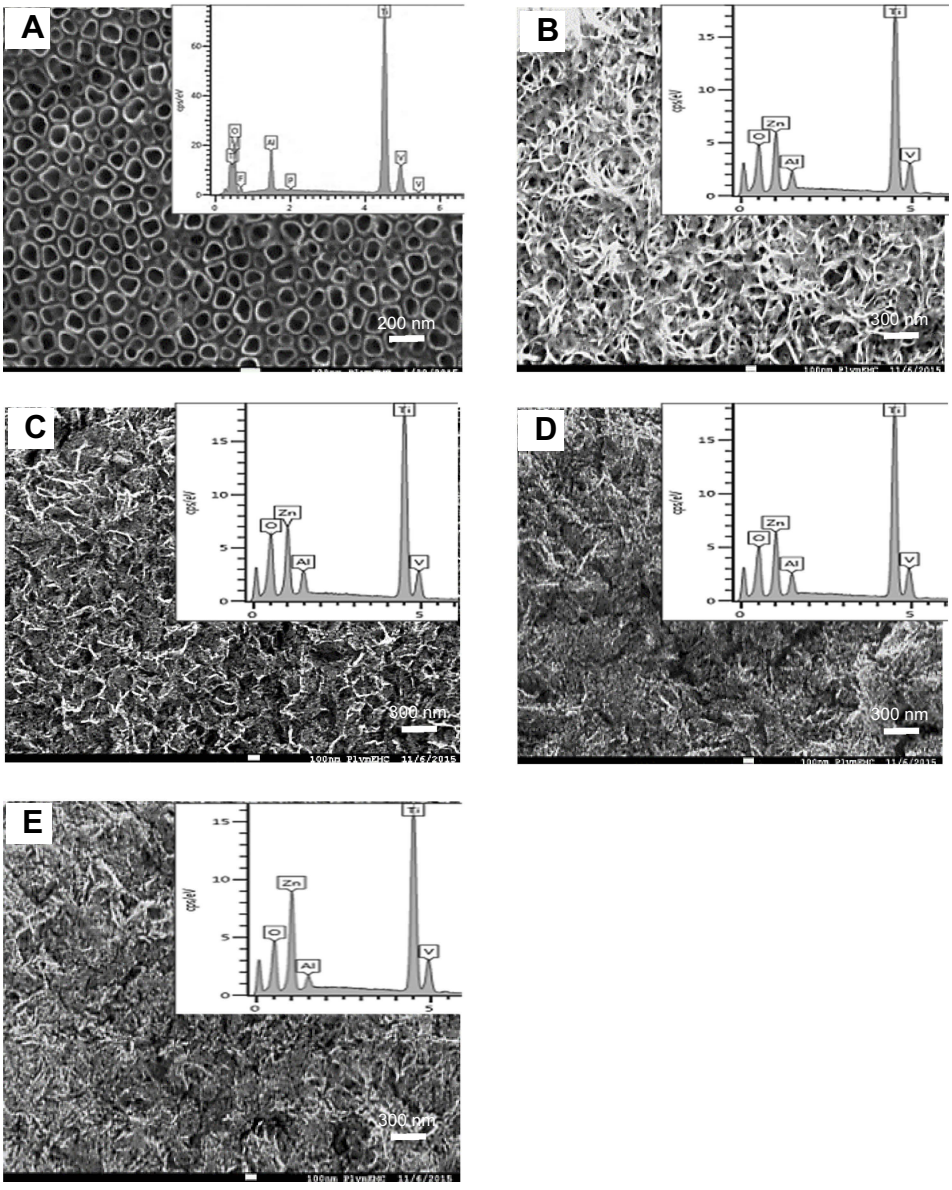

Figure 1 SEM images of Ti alloy surface with (**A**) the self-assembled titania nanotubes (TiO_2 NTs), (**B**) nano zinc oxide (nZnO) grown on the TiO_2 NTs without any heat treatment, and nZnO grown on the TiO_2 NTs after heating to either (**C**) 350 °C, (**D**) 450 °C, or (**E**) 550 °C. There was no hydroxyapatite added to these samples. The inset in each panel shows the elemental composition of the coatings by electron dispersive spectroscopy (EDS). Images are examples from at least three replicates.

any losses of Zn from the discs and the expected decrease of Ca and P in the media during this final step of the HA synthesis. The spent 3SBF media were acidified with 1–2 drops of 70% nitric acid and stored until required for trace metal analysis (see below).

Characterization of the coatings

The morphology and chemical composition of the TiO_2 at each step of the synthesis (ie, addition of nZnO and then HA) were found by SEM with EDS as shown in Figures 1 and 2. Figure 1 shows the surface morphology, prior to the HA additions. The growth of the TiO_2 NTs gave generally good coverage of the alloy. The material is known to consist of two different phases, the alpha-phase (α, the majority of the coating) and the beta phase (β, the depressions), which cause uneven TiO_2 NT growth rate.[39] The additions of nZnO, regardless of the annealing temperature, gave complete coverage (Figures 1B–E), although there were some differences in surface roughness due to heat treatment temperature. Figure 1A illustrates the evenly distributed TiO_2 (before nZnO is added) and the EDS analysis confirmed the chemical composition as mainly Ti and O which is consistent with the presence of a majority of TiO_2. As shown in Figure 1B, TiO_2–ZnO had a nano-needle structure with a length of about 100 nm and width in the order of 10 nm and uniformly distributed over the surface of the nanotubes. The presence of zinc and oxygen in the EDS analysis confirmed the attachment of nZnO to the surface, although the nanostructure of the underlying TiO_2 NTs was visually discernible. Figure 1C illustrates the uniformity of the coating on TiO_2–ZnO/350 with the nano-needle structure still present, but denser than those on TiO_2–ZnO. The EDS analysis showed a higher amount of Zn present on TiO_2–ZnO/350 than on TiO_2-ZnO. Similar observations were made for the TiO_2–ZnO/450 (Figure 1D). However, at the highest annealing temperature of 550 ºC, although the coverage was good (>90% coverage), a few gaps were observed in the coating with respect to TiO_2-ZnO/550 (Figure 1E). The nZnO layer was denser than the other coatings and the underlying nanotubes were not visible. The amount of zinc present on the surface of the TiO_2-ZnO/550 was similar to TiO_2-ZnO/450 by EDS (Figure 1D).

The final completed composite with the HA added is shown in the lower row of Figure 2 (panels A-D). The HA formed on TiO_2 was present as micron-scale globules with nanostructured surfaces as shown in Figure 2A. TiO_2–ZnO, TiO_2–ZnO/350, TiO_2–ZnO/450, and TiO_2–ZnO/550 had HA grown on them after the overnight immersion in 3SBF as seen in Figure 2B–D. With increasing annealing temperature used for nZnO, the HA coating became denser. TiO_2-ZnO-HA/550 (Figure 2E) had less gaps in the coating as compared to TiO_2–ZnO–HA/350 (Figure 2C). The HA coating on TiO_2–ZnO provided a full coverage so that the underlying nZnO was not exposed.

One of the concerns regarding the incubation of the partially made composite in 3SBF was that, while a HA layer might be evolved, this would be at the expense of considerable Zn leaching from the material surface. This was not the case as shown in Figure 3. In Figure 3A, the EDS measurements of the composite before and after incubation in the 3SBF media are shown. While there was a loss of some Zn from the surface as measured by EDS, this was only about one-fifth of the total Zn present regardless of the previous annealing temperature. In terms of total Zn metal lost to the external medium (Figure 3B, one-way ANOVA, $P<0.05$), there was a clear relationship with the annealing temperature in the nZnO addition step, with the highest temperatures resulting in the least Zn leaching. The 3SBF media showed the expected trend of decreasing Ca and P concentrations following the incubation (Figure 3C), consistent with ion adsorption to the surface during HA formation on the composite. The samples at the highest annealing temperature for nZnO coating addition resulted in the greatest decreases in Ca concentration in the 3SBF media (one-way ANOVA, $P<0.05$).

The visual observations of the final surface morphology in Figure 1 were confirmed by surface roughness measurements (Figure 3D). The presence of nZnO on the coating increased the roughness, compared to the TiO_2 nanotubes coating alone (one-way ANOVA, $P<0.05$). The annealing temperature at the nZnO addition step of the synthesis also influenced the final outcome on surface roughness, with the greatest roughness values associated with the highest annealing temperatures (one-way ANOVA, $P<0.05$). However, the final step of HA additions tended to decrease the surface roughness of each composite (one-way ANOVA, $P<0.05$, Figure 3D). In this study, only the coatings were characterized with the aim of testing their antimicrobial activity. The effect of the coatings on the base alloy was not investigated. However, the total coating thickness is below 1 μm so no significant effect on mechanical properties is expected.

For the logistics of biological testing, one "best" composite had to be selected for experimental work. After considering all the characterization information, TiO_2–ZnO/350 and TiO_2–ZnO-HA/350 were chosen as the coated samples to be taken

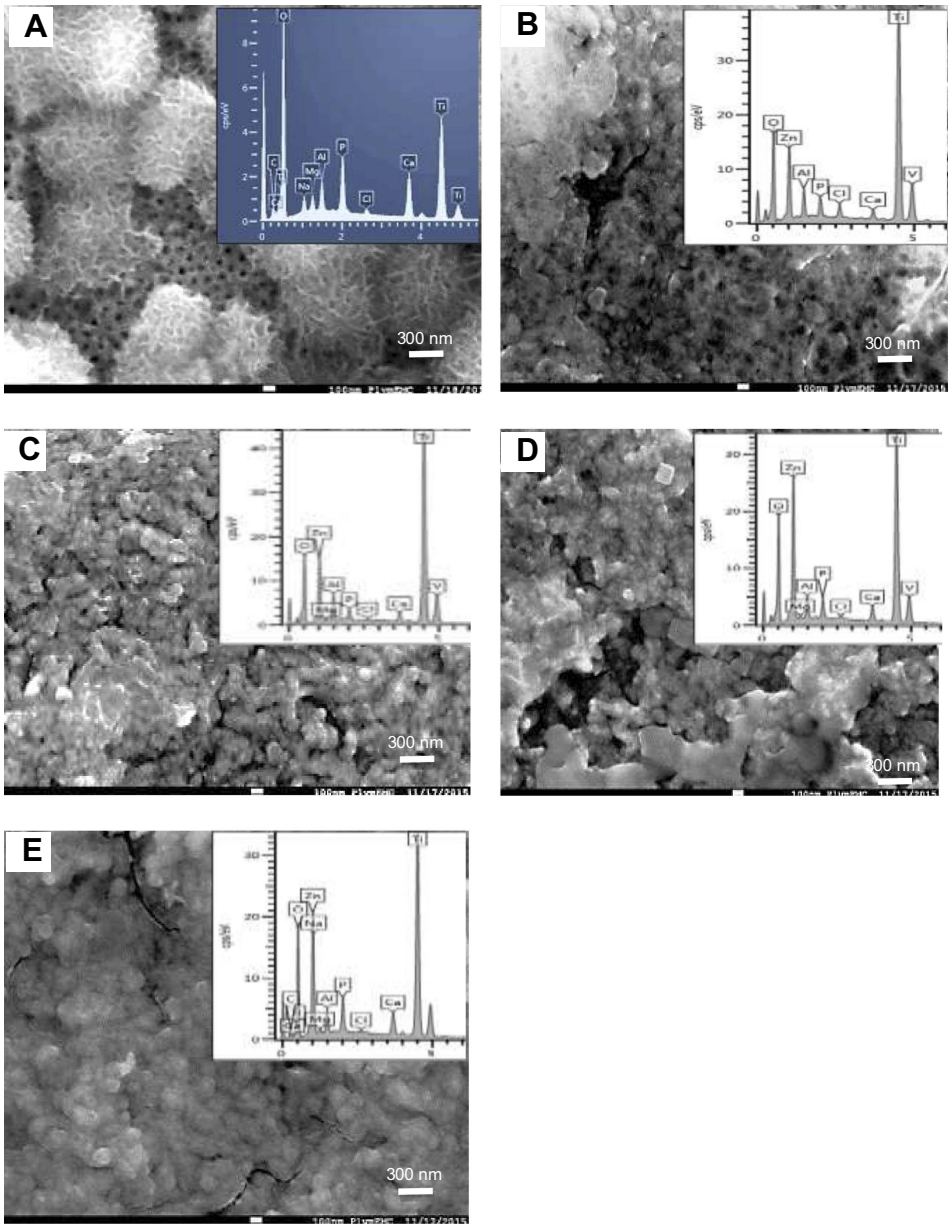

Figure 2 SEM images of HA nanoparticles on top of Ti alloy. (**A**) The self-assembled titania nanotubes (TiO_2 NTs) with hydroxyapatite (HA), (**B**) nano zinc oxide (nZnO) grown on the TiO_2 NTs without any heat treatment, or nZnO grown on the TiO_2 NTs after heating to either (**C**) 350°C, (**D**) 450°C, and (**E**) 550 °C. The inset in each panel shows the elemental composition of the coatings by EDS. Images are examples from at least three replicates.

forward for further testing. This was selected on the basis that the nZnO coating was uniformly structured as well as covering the whole surface, and while the deposition of HA was also good, the gaps in the HA would allow some direct access to the biocidal nZnO coating. Subsequently, further batches of Ti-6Al-4V discs coated with the composite using the 350°C annealing temperature were prepared. The composites were then sterilized under 36.42–40.72 kGy gamma radiation (Becton, Dickinson and Company, Swindon, UK), as we have done previously with nanocoated Ti-6Al-4V alloys.[19]

Dialysis experiment and the release of dissolved metal

This experiment was conducted to aid the interpretation of the biological experiments with respect to the toxicity due to the presence of dissolved Zn, but also to inform on the stability of the coatings in the SBF. The dialysis experiments were conducted according to Besinis et al[44] using the TiO_2–ZnO/350 and TiO_2–ZnO-HA/350 discs as selected for the biological experiments. A normal concentration of SBF was prepared in deionized water,[43] with the pH adjusted to

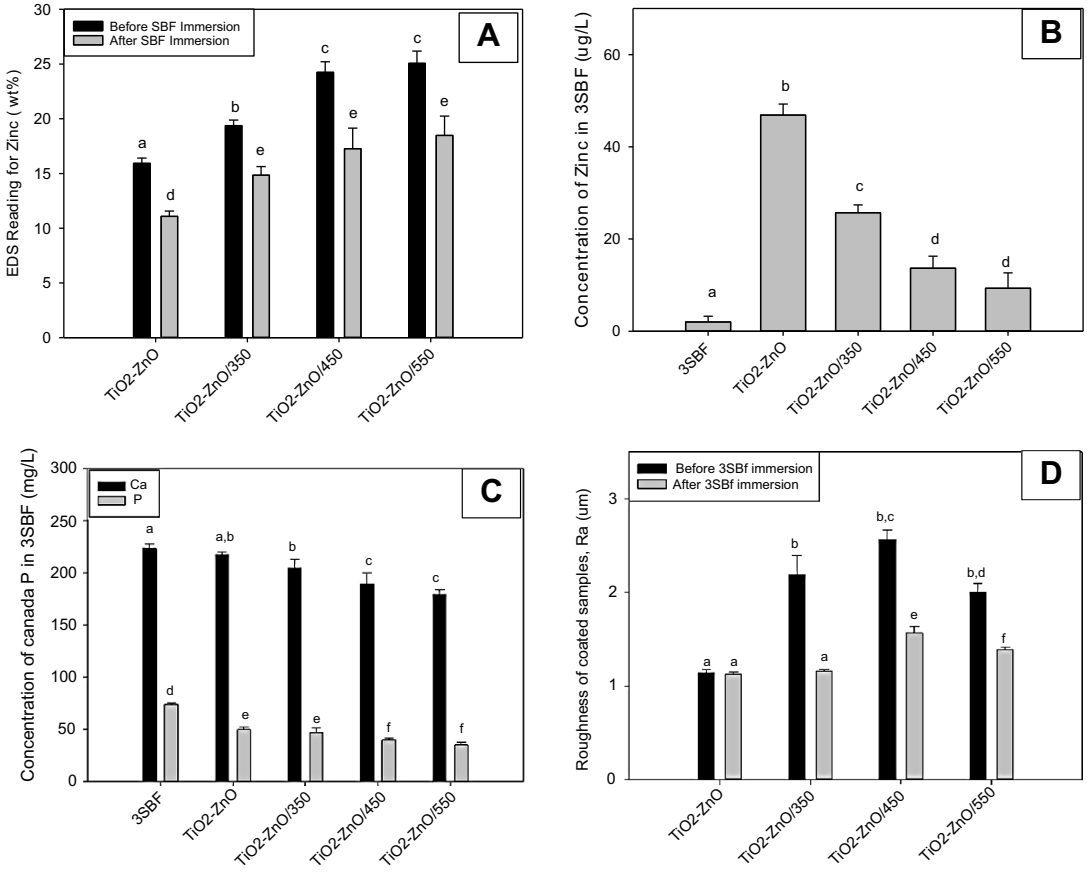

Figure 3 The effect of heat treatment on the composition and the leaching of TiO_2–ZnO coating during the synthesis of the composite coating. (**A**) The total concentration of zinc on the differently heat treated TiO_2–ZnO discs before and after exposure to 3SBF by EDS analysis. (**B**) The total concentration of zinc in the 3SBF measured by ICP-MS after 24 -hr exposure. (**C**) The concentration of total calcium and phosphorus in the 3SBF measured by ICP-MS after 24-hr exposure. (**D**) Surface roughness (Ra values) for the different TiO_2–ZnO coatings before and after immersion in 3SBF, read by Olympus Laser Microscope LEXT OLS3100. Different letters indicate statistically significant differences (ANOVA or Kruskal–Wallis, $P<0.05$) between the type of coating for each measurement. Data are mean ± SEM, n=3 replicates per treatment.

7.4 with a few drops of 1 mol/L HCl. Experiments were conducted in triplicate at room temperature in previously acid washed (5% nitric acid) and deionized glassware. Dialysis tubing (MW cutoff, 12,000 Da, Sigma Aldrich, UK) was cut in 7 cm×2.5 cm lengths and sealed at one end using a Mediclip and then filled with one of the coated discs as appropriate with 7 mL of SBF. The dialysis bag was closed with another Mediclip and the bag suspended in a 500 mL pyrex beaker containing 243 mL of SBF (ie, total volume 250 mL). The beakers were gently stirred throughout and maintained at 37°C, and 4 mL aliquots of the SBF was collected from the external compartment of the beaker at 0, 0.5, 1, 2, 3, 4, 6, 8, and 24 hrs. The SBF samples were acidified with a drop of 70 wt% nitric acid and stored for metal analysis (see below). At the end of the 24 hrs, the dialysis bags were also carefully opened and 4 mL of the fluid therein collected for metal analysis. Dialysis curves were plotted using SigmaPlot 13.0 (Systat Software, Inc.), after deducting the background ionic concentrations of the SBF. A first-order rectangular hyperbola function was used to fit dialysis curves to the raw data. The maximum initial slope of the curves informed on the maximum apparent dissolution rate of each substance.

Plate preparation and exposure to *S. aureus*

The experimental design involved exposing *S. aureus* to the coated samples of TiO_2–ZnO/350 and TiO_2–ZnO-HA/350 in 24-well, flat-bottom sterile polystyrene plates (Thermo Fischer Scientific, Loughborough, UK). TiO_2 NT-coated discs were used as a control for the coating effect. Zinc chloride was used as a metal salt control for any possible dissolved zinc effect from the nZnO. *S. aureus* was allowed to grow on its own as a negative control (ie, no biomaterials present). Nine replicate runs were conducted for each type of coated samples and the various controls (n=6 for biochemical assays and n=3 for SEM). Following the approach

by Besinis et al,[44] the materials were exposed to *S. aureus* for 24 hrs and the proportion of live to dead cells and the amount of lactate produced were evaluated (see below). The concentration of total dissolved zinc, calcium, and phosphorus released from the coating in the SBF was also measured (see metal analysis, below).

S. aureus was chosen as it is considered to be one of the main causes of infection in orthopedic and dental implants.[38,45] *S. aureus* was cultured in brain heart infusion (BHI) broth (Lab M Ltd, Bury, UK) at 37°C. A bacterial suspension having OD 0.018 at 595 nm absorbance (Spectrophotometer Genesys 20, Fisher Scientific) was prepared in the BHI broth at a concentration of 1×10^7 cells/mL. For the experiments, 2 mL of the bacterial culture was pipetted in each well of a 24-well plate containing TiO_2 NTs, TiO_2–ZnO/350, TiO_2–ZnO–HA/350, $ZnCl_2$ (0.001 M), and nZnO dispersed in ultrapure deionized water on their own (n=9 replicates of each). A zinc concentration of 0.001 M was used for the positive controls as this reflected the maximum amount of zinc released from the coatings. The 24-well microplates were then incubated at 37ºC on a shaking table. At the end of the overnight exposure, six of the replicate plates were used for biochemistry. An aliquot (1 mL) of the supernatant from each well was collected for the LIVE/DEAD® kit and lactate production assays (see below). The remaining supernatant was acidified with 70 wt% HNO_3 and used for metal determination. Then, the remaining adherent bacterial pellets were collected. Bacterial pellets were obtained using the same protocol as Besinis et al,[19] whereby the samples from the wells were sonicated (12 MHz) for 60 s in 2 mL of sterile saline to remove the attached bacteria from the discs. Then, 1 mL of the resulting suspension was allowed to grow in 5 mL of BHI broth for 5 hrs at 37ºC on a shaking table with the aim of increasing the amount of live cells in order to readily measure them with the Live/Dead assay. The viability of the cells and the amount of lactate in the suspension was also assessed followed by the measurement of the ionic composition of the latter. For the remaining three replicates, the supernatant was removed and the samples were prepared for electron microscopy (see below).

Cell viability

The cell viability of *S. aureus* in both the supernatant and incubated cell suspension from all of the relevant treatments and controls were assessed using the L7012 LIVE/DEAD® Backlight™ Kit (Invitrogen Ltd, Paisley, UK). Briefly, 100 µL of the supernatant and 100 µL of the incubated homogenate from each replicate for the different treatments were transferred to a V-bottom 96-well microplates (Corning, UK). The microplates were centrifuged at 4,000 rpm for 10 mins in a 2,040 Rotors microplate centrifuge (Centurion Scientific Ltd, Chichester, UK) with the aim of pelleting the bacteria, after which the pellets in each well were washed with 1 mL of sterile NaCl saline. The pellets were centrifuged again at 4,000 rpm for another 10 mins. The final washed pellets were resuspended in 1 mL of saline. Then, 100 µL of the final suspension from each well was pipetted into another 96-well plate flat bottom microplate for fluorimetry. Briefly, 100 µL of freshly prepared dyes from the LIVE/DEAD kit was added to those wells and mixed thoroughly. The microplate was incubated in the dark at room temperature for 15 mins after which the fluorescence of the wells was immediately measured on a Cytofluor II fluorescence plate reader (PerSeptive Biosystems, Inc., Framingham, MA, USA) at an excitation wavelength of 485 nm and emission wavelengths of 530 nm and 645 nm, respectively. The readings at 530 nm were divided by the readings at 645 nm in order to obtain the percentage of live to dead cells in the supernatant and the incubated cell suspension from the different samples and controls according to the kit instructions.

Lactate production

The metabolic activity of *S. aureus* was assessed by measuring the amount of lactate present in both the supernatant and incubated cell suspension from the treatments and appropriate controls in the experiment (6 replicates of each) using the approach utilized by Besinis et al.[44] The measurement of lactate would suggest the presence of metabolically active bacterial cells. The lactate assay reagent was prepared by pipetting 1 µL of 1,000 units/mL of lactate dehydrogenase (Sigma-Aldrich Ltd, St. Louis, MI, USA) into wells in a flat-bottom 96-well plate followed by 10 µL of 40 mmol/L nicotinamide adenine dinucleotide (NAD) (Melford Laboratories Ltd, Ipswich, UK) and 200 µL of 0.4 mol/L hydrazine prepared in a glycine buffer of pH 9. Then, 100 µL of the supernatant, or 100 µL of the incubated homogenate as appropriate, was transferred to a V-bottom 96-well microplate and centrifuged at 2,000 rpm for 10 mins to generate a clean supernatant that could be measured for total lactate. 10 µL of these supernatants was added to the 211 µL of the lactate assay reagent mixture in the flat-bottom 96-well plate described above. The microplate was then placed in an incubator at 37ºC for 2 hrs to allow lactate production to occur. The absorbance was then read at 340 nm against

lactic acid as standards (0, 0.25, 0.5, 1.0, 2.0, 4.0, and 8.0 mmol/L).

Metal analysis following *S. aureus* exposure

The exposed broth and the detached bacteria were analyzed for zinc, calcium, and phosphorus composition. After the exposure to *S. aureus*, 1 mL of the broth or the detached bacteria was diluted with Milli-Q water to a final volume of 5 mL. Subsequently, they were acidified with two drops of 70 wt% nitric acid to prevent Zn adsorption to the test tubes during storage. Total Zn concentrations were determined by inductively coupled plasma mass spectrometry (ICP-MS, Varian 725-ES Melbourne, Australia). Whereas the total Ca and P concentrations were analyzed by optical emission spectrometry (ICP-OES, Thermo Scientific XSeries 2, Hemel Hempstead, UK). Calibrations for both ICP-OES and ICP-MS were performed with matrix-matched analytical grade standards. For ICP-MS, the standards and samples contained internal references (0.5%, 0.25%, and 1% of iridium) for SBF, broth and any homogenates made from bacteria. In the complex matrix of broth and SBF, the detection limit was around 0.003 μg/L for zinc for ICP-MS and 5 μg/L for calcium and 40 μg/L for phosphorus by ICP-OES.

Imaging of the attached *S. aureus*

The remaining 3 repeats of the control, TiO_2, TiO_2–ZnO/350, TiO_2–ZnO–HA/350, $ZnCl_2$ and nZnO alone were used for imaging under high-resolution SEM with the aim of visually confirming the attachment of *S. aureus* on the different surfaces. After the 24-hr exposure to *S. aureus*, the supernatants from the 24-well plates were removed after which the plates were washed twice with sterile saline (0.85 wt% NaCl). Then, 2 mL of 3 wt% glutaraldehyde in 0.1 mol/L cacodylate buffer was added to each well and was allowed to stay overnight at 4ºC. The next day, the glutaraldehyde was removed, and the samples were washed with 0.1 mol/L cacodylate buffer. An increasing concentration of ethanol (30%, 50%, 70%, 90%, and 100%) was used for serial dehydration of the samples as appropriate. The samples were then coated with carbon for viewing under a JEOL7001F SEM. Once in the microscope vacuum chamber, each sample was viewed at three different random locations (ie, 3 images of each specimen ×3 replicate samples). Care was taken to systematically photograph the specimens at the same magnifications. A ×1,000 magnification was used to explore the extent of coverage of the surface with *S. aureus*.

Statistical analysis

The data from the cell viability assay, the lactate production assay, and the ionic concentration measurements were analyzed using Statgraphics Centurion XVII (StatPoint Technologies, Inc.). After descriptive statistics, data were checked for normality and for equal variances (Levene's test). When data were parametric, the data were analyzed for treatment or time effects using one-way ANOVA with Fisher's least significant difference (LSD) test post-hoc. In cases of unequal variances, the data were transformed before analysis and where the data remained nonparametric, the Kruskal–Wallis test was used. Data are presented as mean ± SEM unless otherwise stated. The default 95% confidence level was used for all statistics.

Results

Dialysis experiment and the stability of coatings

Prior to the analysis of the release of zinc from the coatings in the presence of the *S. aureus* (see below), the dissolution of apparent total Zn from the coatings were analyzed in the presence of SBF to aid the interpretation of the bioassays and to inform on the stability of the coatings. The results are reported in Figure 4. The total concentration of Zn in the beakers from the samples without any added zinc was minimal, as expected. For the coatings containing Zn, there was an exponential rise in the total Zn concentration in the external compartment of the dialysis bag, reaching a maximum total Zn concentration of 8.17±0.42 μg/L and 4.24±0.36 μg/L from TiO_2–ZnO/350 and TiO_2–ZnO–HA/350, respectively. The maximum dissolution rates were 4.35±0.17 μg/hr and 2.60 ±0.19 μg/hr for Zn from ZnO/350 and TiO_2–ZnO–HA/350, respectively. The dissolution rate from TiO_2–ZnO/350 was significantly higher than that from TiO_2–ZnO–HA/350 (one-way ANOVA, $P<0.05$, n=3). It was also observed that the discs were not exhausted of Zn as Zn was measured inside the dialysis bag at the end of the experiment, and the resulting concentrations were 9.42±1.20 μg/L and 6.78±1.56 μg/L from TiO_2–ZnO/350 and TiO_2–ZnO–HA/350, respectively.

Figure 4 also showed the dissolution of calcium and phosphorus from the coated samples. Similar saturation mode in the total concentrations was observed for both Ca

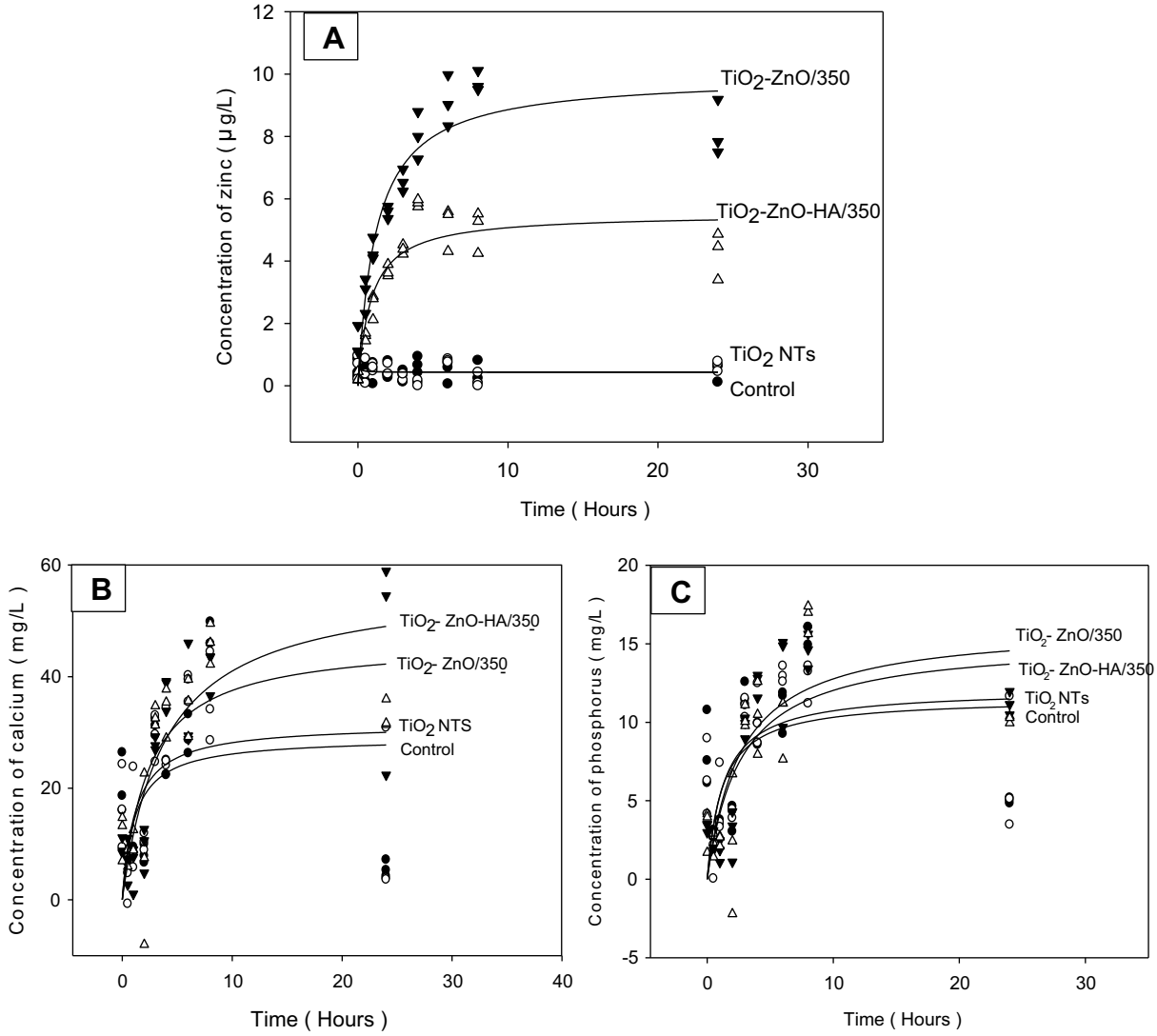

Figure 4 Dialysis of titanium alloy discs coated with either TiO_2 NTs (• Symbol), TiO_2 NTs decorated with nZnO (TiO_2–ZnO/350, ▼Symbol), or also with hydroxyapatite (TiO_2-ZnO-HA/350, Δ Symbol) in simulated body fluid (1× SBF). Concentration of (**A**) total zinc measured by the ICP-MS, (**B**) total calcium, and (**C**) total phosphorus measured by the ICP-OES, in SBF from the dialysis in the external compartment of the beakers. Data are single values from triplicate beakers. The curves were fitted to the raw data using a rectangular hyperbola in SigmaPlot.

and P in the beakers (Figure 4B and C). The maximum concentration of Ca reached was 105.27±9.40 mg/L and 93.00±1.21 mg/L from TiO_2–ZnO/350 and TiO_2–ZnO–HA/350, respectively, with a maximum dissolution rate of 65.89 ±2.00 mg/hr and 70.12±0.98 mg/hr, respectively. The maximum concentration of P reached was 31.20±0.35 mg/L and 30.21±0.11 mg/L from TiO_2–ZnO/350 and TiO_2–ZnO–HA/350, respectively, with a maximum dissolution rate of 21.79 ±0.33 mg/hr and 22.50±0.17 mg/hr, respectively. At the end of the experiment, the concentrations of Ca and P in the dialysis bag were 85.09±1.04 mg/L and 27.02±0.53 mg/L for TiO_2–ZnO/350 and 82.85±2.28 mg/L and 25.80±0.71 mg/L for TiO_2–ZnO–HA/350, respectively.

Confirming zinc release in the broth during *S. aureus* exposures

The measured total Zn concentrations in the broth during the exposure of *S. aureus* to the different composite coating and relevant controls are shown in Figure 5A. For the controls and materials without added zinc, as expected they showed only a background concentration of the metal (around 1.4 µg/L). The positive controls of $ZnCl_2$ and nZnO, as expected, showed a high concentration of zinc: 405±11.3 µg/L and 354 ±7.16 µg/L, respectively. Where the coatings contained nZnO, total Zn (form unknown) was readily measured in the broth (Figure 5A). The broth exposed to both TiO_2–ZnO/350 and TiO_2–ZnO–HA/350 discs had 45.0±7.2 and

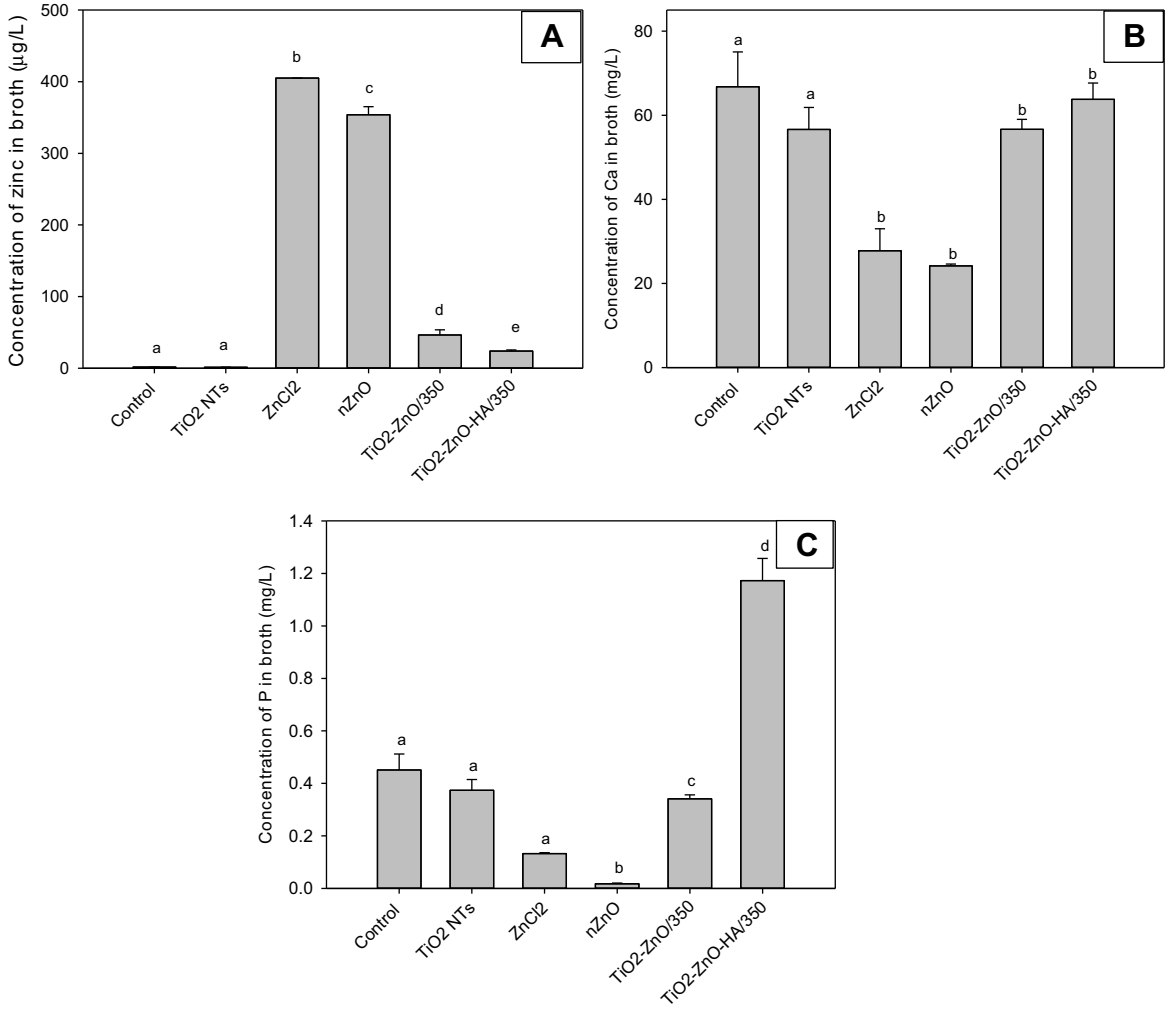

Figure 5 Total concentration of (**A**) zinc, (**B**) calcium, and (**C**) phosphorus, in the exposed broth after 24-hr growth of *S. aureus* in controls (cell culture plate without any titanium alloy disc), on TiO_2 NTs, in the presence of $ZnCl_2$ or a dispersion of nZnO particles alone, or TiO2 NTs decorated with nZnO (TiO_2–ZnO/350), or also with hydroxyapatite on the coating (TiO_2–ZnO–HA/350). Zinc was measured by ICP-MS and Ca and *P* by ICP-OES for zinc. Different letters indicate statistically significant differences (Kruskal–Wallis, $P<0.05$) between the type of coating for each measurement. Data are mean ± SEM, n=6 replicates per treatment.

22.6±0.9 µg/L of total Zn, respectively, with significantly less total Zn from the latter coating with HA (Kruskal–Wallis, $P<0.05$; n=6). This suggests the HA coating is impeding the release of total Zn into the media, but nonetheless, this was still enough to be biocidal (see Cell morphology and survival section).

Cell morphology and survival

Specimens from the controls and treatments were examined for abundance and morphology of the bacteria by electron microscopy at the end of the experiment, and the resulting surface is reflected in Figure 6. The bacteria in the wells without any discs in them (ie, a control grown directly on the plastic of the culture plate) survived and grew on the whole surface of each well, as expected (Figure 6A). The bacteria cultured on the TiO_2 NT discs also grew over the whole surface of the discs, although slightly less dense than the plastic control (Figure 6B). In contrast, the treatments with either just the zinc salt (Figure 6C) or ZnO alone (Figure 6D) showed very few bacteria, indicating that both treatments were very biocidal. The discs coated with both TiO_2–ZnO/350 and TiO_2–ZnO–HA/350 also had much reduced coverage of bacterial cells attached to their surfaces compared to the discs coated with just TiO_2 NTs, showing that the composites with or without the HA present retained antimicrobial properties.

Electron microscopy alone can only determine the presence of bacteria, not whether the organisms are alive or dead. The viability of *S. aureus* was therefore analyzed using the L7012 LIVE/DEAD® Backlight™ Kit after 24

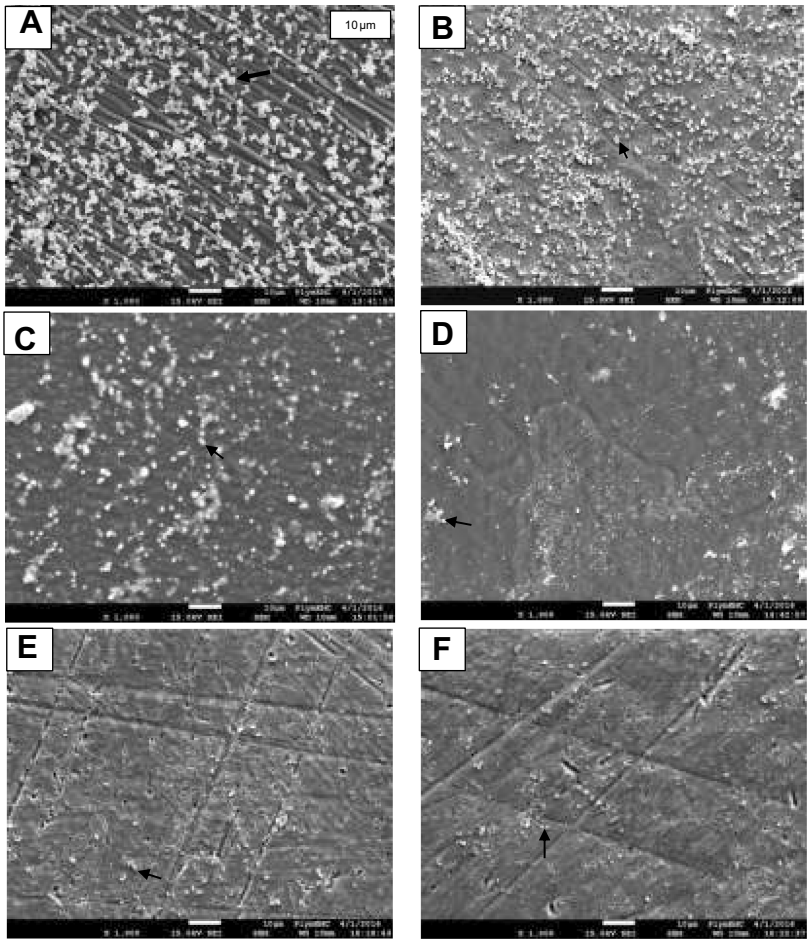

Figure 6 SEM images of attached *S. aureus* (white structures; examples showed by arrow) after 24-hr culture (**A**) controls (cell culture plate without any titanium alloy disc), (**B**) on titanium alloy with TiO_2 NTs, (**C**) in the presence of $ZnCl_2$, or (**D**) a dispersion of nZnO particles alone, (**E**) titanium alloy with TiO_2 NTs and decorated with nZnO (TiO_2–ZnO/350), or (**F**) also with hydroxyapatite on the coating (TiO_2–ZnO–HA/350). Images are representative micrographs from at n=3 replicated samples (scale the same for all images).

hrs of exposure to the composite materials or the appropriate controls. Bacterial cell viability was determined for the bacteria firmly attached to the substrate (Figure 7A) and those still present in the overlying broth (Figure 7B). The lactate production by the bacteria was also measured in homogenates from the biofilm (Figure 7C) and from bacteria in the overlying media (Figure 7D) to confirm that the cells had some metabolic activity. Overall, the results of the LIVE/DEAD assay and lactate production (Figure 7) reflected the morphological observations (Figure 6). In the unexposed control, as expected for plastic culture wells and in keeping with the electron microscopy observations, the attached biofilm had excellent viability (mean ± SEM, n=6) of 100±3% and less in the cells in the overlying broth (72±3%, statistically different, Kruskal–Wallis, $P<0.05$, n=6). Both the attached cells and those remaining suspended in the broth showed readily measurable lactate production (Figures 7C and D), with more in the attached microbes, as expected (Kruskal–Wallis, $P<0.05$, n=6). The survival of bacteria attached to TiO_2 NTs (63±3%), or in the broth overlying the TiO_2 NTs (38±2%), had slightly less viability than the plastic plate controls (statistically significant for each, Kruskal–Wallis, $P<0.05$, n=6), but both showed similar lactate production to their respective controls. This indicated that the cells observed on the TiO_2 NTs (Figure 6) were mostly alive and metabolically active. In contrast, most of the bacteria in the overlying broth, from either the zinc salt or zinc oxide nanoparticles alone, were dead (6±2% and 2±0% alive, respectively), and this was reflected in low lactate production (Figure 7D). The attached cells from the $ZnCl_2$ treatment fared better with 50±2% survival, but those from the nZnO treatment did not (only 1% survival, Figure 7A), indicating a higher biocidal activity by nZnO than $ZnCl_2$.

The discs coated with both TiO_2–ZnO/350 and TiO_2–ZnO–HA/350 were also very biocidal, although not as effective as $ZnCl_2$ or nZnO alone (Figure 7). The bacterial

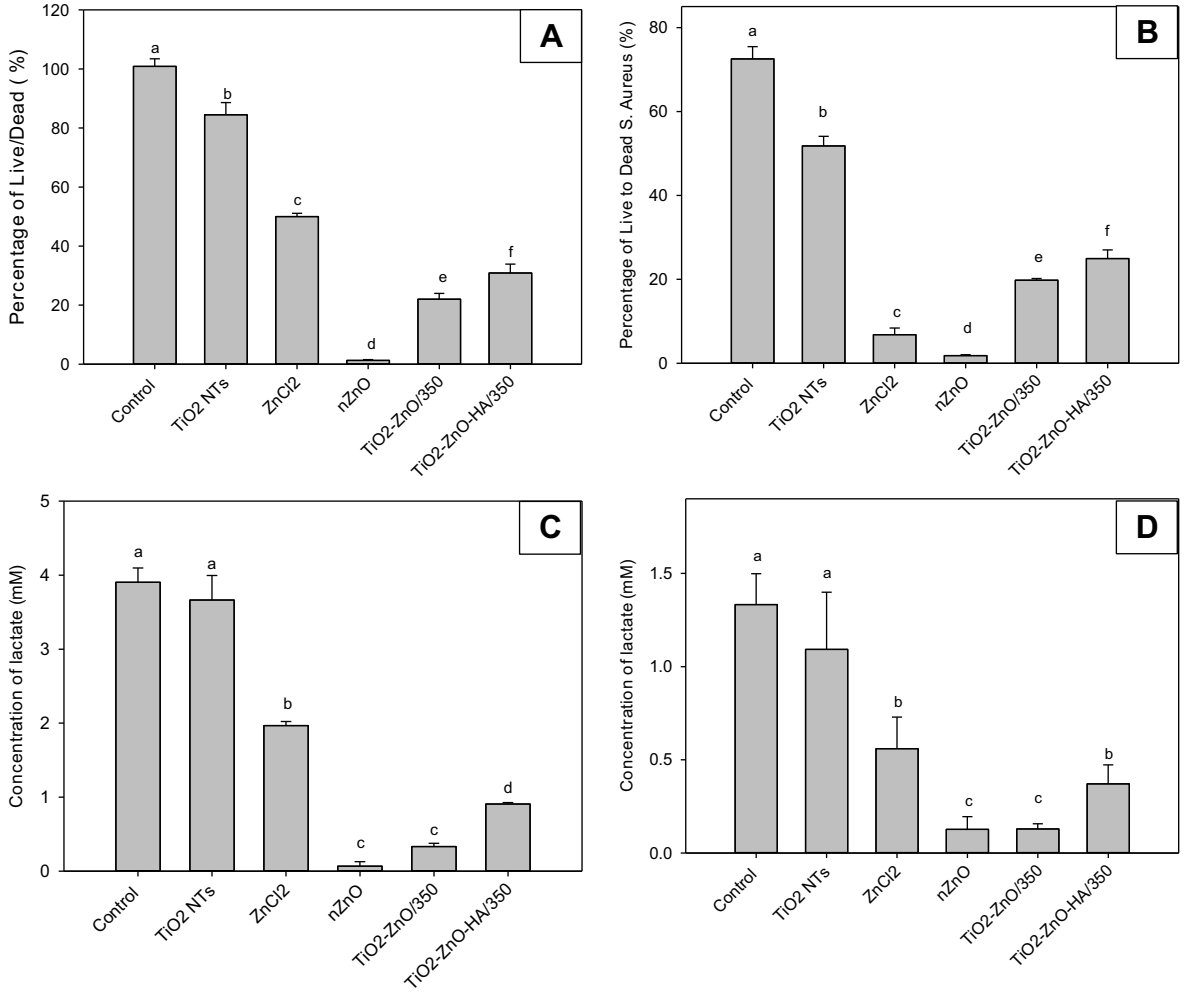

Figure 7 Percent survival (upper panels) and lactate production (lower panels) by *S. aureus* grown overnight in BHI broth at 37°C, on controls (cell culture plate without any titanium alloy disc), on TiO_2 NTs, in the presence of $ZnCl_2$ or a dispersion of nZnO particles alone, or TiO_2 NTs decorated with nZnO (TiO_2–ZnO/350), or also with hydroxyapatite on the coating (TiO_2–ZnO–HA/350). Panels (**A**) and (**C**) are for bacteria attached to the relevant substrate and panels (**B**) and (**D**) for microbes remaining suspended in the overlying broth. Different letters indicate statistically significant differences (Kruskal–Wallis, $P<0.05$) between treatments for each measurement. Data are mean ± SEM, n=6 replicates per treatment.

cells on the TiO_2–ZnO/350 and TiO_2–ZnO–HA/350 were mostly dead, with only 22.0±2.0% and 30.9±3.0% of live to dead cells, respectively (Figure 7A). This was significantly lower than those cells alive on the TiO_2 NT discs (Kruskal–Wallis, $P<0.05$, n=6), confirming that the presence of nZnO in the coatings was killing the bacterial cells. Similar observations were made for surviving cells in the overlying broth in the TiO_2–ZnO/350 and TiO_2–ZnO–HA/350 treatments (Figure 7B). The moderately low survival was also reflected in the lactate production by the attached bacteria on the surface of TiO_2–ZnO/350 and TiO_2–ZnO–HA/350; values were 0.13±0.03 mM and 0.37±0.1 mM, respectively, which were significantly lower (Kruskal–Wallis, $P<0.05$, n=6) than that produced by the bacteria on TiO_2 NTs (1.1±0.3 mM lactate, Figure 7C). Indeed, in terms of lactate production by either the attached biofilm, or the overlying broth, the TiO_2–ZnO/350 discs were as effective as nZnO alone (Kruskal–Wallis, $P>0.05$, n=6). The addition of HA was less effective, with the TiO_2–ZnO–HA/350 treatments showing a little more lactate production in the attached biofilm, but this was still much inhibited compared to either the unexposed controls or the TiO_2 NTs alone (Figure 7C).

Discussion

Overall, this study aimed to make a biomaterial that was durable and capable of being decorated with nano-HA to impart potential biocompatibility with human bone. Both these features were considered with the safety requirements of medical implants in mind. The material was also designed to offer antimicrobial properties by the addition of zinc. This was achieved by using TiO_2 NTs as a scaffold to grow nZnO, and

the subsequent annealing ensured that the nZnO particles remained attached. The material, with or without HA present, showed a slow and beneficial dissolution of Zn in SBF, that was also biocidal to one of the pathogens known to be a concern during implant surgery, *S. aureus*. The biocidal nature was confirmed by poor coverage of bacteria on the biomaterial and reduced bacterial survival as well as low lactate production by those microbes remaining.

Advantages and stability of ZnO nanocoatings

Although TiO_2 NTs on the surface of titanium alloy have been successfully used as a platform for the attachment of antibiotics to deliver some antimicrobial properties to bone implant material,[46] this approach is problematic because the antibiotics, as organic compounds, will inevitably be degraded, and thus offer only transient protection. There is also the concern of antibiotic resistance. The approach here, to use Zn as a biocide, therefore offers some advantages. An initial concentration of 0.075 mol/L of zinc nitrate as the source of zinc and 0.1 mol/L of hexamethylenetetramine successfully yielded nZnO particles on the surface of TiO_2 NTs (Figure 1). The morphology of the TiO_2 NTs and the decoration with nZnO were similar to those reported by Liu et al[42] using the same concentration of zinc nitrate. In the latter study, the resulting nZnO had a thinner structure, compared to those in the present study where the annealing modified the morphology of the as-grown ZnO nanocoating to a more spherical shape and altered the size of the nZnO (Figure 1). The ability of annealing temperatures to alter the size of nZnO has been reported previously[33] and was associated with the alteration in the crystal size and the reduced number of vacancies in zinc in the annealed zinc oxide. The annealing process is intended to improve the bonding of the nZnO (and any subsequent HA) to the relevant substrate as well as influence the size of the resulting crystals. Increasing the temperature has also been shown to improve the stoichiometry of the nZnO crystals,[33] in this study, a temperature higher than 350ºC caused the crystals of nZnO to merge with each other, reducing the porous structure of the latter coating (Figure 1). This change, in turn, resulted in bigger crystals of HA forming on the surface of the nZnO (Figure 2). This might be regarded as clinically beneficial for a bone implant material, as better HA coverage is known to increase biocompatibility with osteoblasts.[47] There was also some loss of Ca and P from the 3× concentrated SBF in the presence of the coatings (Figure 3), and this is likely due to adsorption to the coating surface and may, in the case of HA, also contribute to crystal growth. However, the Ca and P were also labile, and in the dialysis experiments with freshly prepared SBF, some Ca and P were leached into the medium (Figure 4).

Regardless of the detailed mechanisms involved in crystal formation, the resulting TiO_2–ZnO and TiO_2–ZnO–HA combinations with an annealing temperature of 350ºC were selected for antimicrobial testing, partly on the basis of the results from the incubations in SBF (Figure 3). These experiments confirmed that μg/L concentrations of total Zn were released from the coating in SBF, and of the annealing temperatures used, 350°C achieved the best release (Figure 3B), but with much of the original Zn remaining on the coating, as measured by EDS (Figure 3A). This indicated a slow release of zinc into a biologically relevant media, whilst maintaining the coating integrity in terms of elemental composition and surface roughness. The cause of the apparent total Zn release into the SBF, in theory, could either be due to slight erosion of the coating such that intact nZnO particles were being released into the media, or more likely, the release of dissolved Zn ions by dissolution of the nZnO particles attached to the TiO_2 NTs. The dialysis experiments (Figure 4) confirmed the latter. The dialysis tubing (measured pore size <2 nm) enables only the apparent soluble Zn fraction to diffuse into the external compartment of the beakers, and this achieved equilibrium following a rectangular hyperbola as expected for solutes (Figure 4). The dissolution of nZnO particles in biological fluids is well known, and nZnO is sparingly soluble such that usually a few μg/L of Zn^{2+} ions is released over 24 hrs, depending on the details of the material synthesis and media composition.[48] Similarly, in SBF, μg/L concentrations of apparent total dissolved Zn were released during the dialysis experiments (Figure 4). Less Zn was released by dissolution from the TiO_2–ZnO–HA/350 coating as compared to the TiO_2–ZnO/350 coating, likely because the HA top coat was limiting the accessible area of the nZnO for the media. Nonetheless, even in the presence of HA on the coating, the maximum release rate of total Zn was 2.6 μg/hr and is broadly comparable to other biocidal nanomaterials such as Ag NPs.[44] This release of Zn was biocidal to *S. aureus* (see Antibacterial properties section).

Antibacterial properties

TiO_2 NTs on medical grade titanium alloy provide a nanoscale surface that may better support osseointegration of bone implant compared to titanium alloy alone, but the TiO_2 NTs do not have any inherent antibacterial properties.[42,49] This was also the case in the present study, and although *S. aureus* grew less well on TiO_2

NTs compared to directly on the cell culture plate, there was still >80% viability of the bacteria and with no effects on lactate production (Figure 7). In contrast, both the positive control of 1 mmol/L $ZnCl_2$ and the nZnO particles alone were effectively killing the bacteria (Figure 7). The toxicity of $ZnCl_2$ to *S. aureus* is expected, with 2 mmol/L of Zn or much less reported to cause complete growth inhibition, depending on the strain of organism used,[50] and zinc is generally biocidal to microbes in the 1–10 mmol/L range, depending on salinity and temperature.[51] Zinc oxide nanoparticles have also been shown to effectively inhibit the growth of microbes such as *E. coli* and *S. mutans*.[23,24,42] There are fewer reports of nZnO toxicity to *S. aureus*, although concentrations of around 100 mg/L of nZnO are reported to cause growth inhibition.[52] Nonetheless, in the experimental conditions used here, the measured 354 µg/L of Zn as nZnO in the broth was an effective biocide (Figures 6 and 7) and was more effective than the $ZnCl_2$ treatment (Figure 7). The mechanism by which nZnO causes toxicity to microbes is not fully understood, but could involve free ion toxicity derived from the dissolution of the metal ion, or by direct contact toxicity of the particle on the exterior surface of the microbe, as has been suggested for Ag NPs.[53] The dialysis experiments confirmed dissolution of Zn (Figure 4), and hence Zn was detected in the SBF (Figure 3).

However, the key concern was whether or not nZnO was toxic to the microbes when present in the coating. Both the TiO_2–ZnO/350 and TiO_2–ZnO–HA/350 coatings caused growth inhibition of *S. aureus*. There were less coverage of bacteria on these coatings (Figure 6) and fewer live bacteria present (Figure 7) compared to the TiO_2 NTs coating alone. About 80% of the bacterial cells died in the presence of TiO_2–ZnO/350 (Figure 7B). This is in agreement with the findings of Liu et al[42] and Roguska et al[29] in similar studies with nZnO coatings. However, in the present study, the distribution of the nZnO was more uniform and more stable due to the annealing process and arguably making the coating more efficient. Regardless, the addition of nano-HA on the nZnO slightly reduced the antibacterial effect of the coating. This might be expected, as the HA provides a barrier that could prevent direct contact of the bacteria with the underlying nZnO. For example, the gaps in the HA coverage were of the order of 200–300 nm at most (Figure 2), and yet the bacteria are around 2 µm long (Figure 6). The addition of HA did reduce the Zn dissolution from the coating (Figure 4), perhaps because the exposed surface area of nZnO was less. The chemical reaction between HA and nZnO also has to be taken into consideration, as zinc can attach or be adsorbed onto the HA particle, and hence decreases the apparent Zn leaching from the coating.[54] However, the small gaps in the HA structure did allow some Zn dissolution (Figure 4) and with a maximum dissolution rate of 4.35 µg/hr. The latter would roughly equate to a release about 100 µg of Zn into a small volume (a few milliliters) around the point of surgery in a patient. Given the MIC for dissolved Zn is around 1 mmol/L (or 65 µg/mL), this would represent a desirable slow release of antibacterial Zn in the patient during and immediately after surgery, when the infection risk is greatest.

However, the coating containing nZnO did not completely kill the bacteria. The TiO_2–ZnO–HA/350 caused about 60% mortality of the bacteria present on the coating (Figure 7A). Other cations in the media, such as calcium, can compete with dissolved zinc for uptake into cells,[55] and the relatively high cation concentrations in the SBF may have offered the bacteria some protection from Zn exposure. The nZnO coating was also much less effective as a biocide than Ag NPs attached to TiO_2 NTs. For example, on the same TiO_2 NTs used here, Gunputh et al[56] showed the addition of Ag NPs killed >90% of the *S. aureus* present. This is not surprising, with the exceptional toxicity of Ag being associated with its ability to bind to –SH groups in proteins,[53] and being a non-essential metal there is no endogenous ion transport system in microbes to regulate intracellular concentrations of silver or prevent bioaccumulation. These same features of Ag make it less desirable for use in patients compared to zinc. Clearly, the moderate biocidal properties of nZnO coatings need to be considered with the benefits of Zn as an essential metal which is inherently less hazardous than silver for humans in the long term.

Conclusions

In conclusion, a composite coating was successfully synthesized with a uniform distribution of nZnO on TiO_2 NTs. The coating appeared stable in SBF over 24 hrs, and the dialysis experiments showed a slow, beneficial release of dissolved Zn. The addition of nano-HA maintained the roughness and nanostructure of the coating, but still enable an antimicrobial Zn release from the material, which was effective at killing around 60% of *S. aureus* attached to the coating. Further work is needed to confirm the antibacterial properties of the coatings against other common causes of orthopedic/dental implants infections such as *Streptococcus mutans and E. coli*, understanding the biocompatibility of the coating with human osteoblasts and whether less HA can be used to further improve

access to the antimicrobial nZnO in the coating.

Acknowledgments

The authors would like to acknowledge the funding through a joint PhD studentship for UG by the Faculty of Science and Environment and Peninsular Schools of Medicine and Dentistry. The assistance by the technical team in the School of Marine Science and Engineering, the School of Biological and Biomedical Science, and the Electron Microscopy Centre (EMC) of Plymouth University is gratefully acknowledged.

Disclosure

The authors report no conflicts of interest in this work.

References

1. O'Brien FJ. Biomaterials & scaffolds for tissue engineering. *Mater Today*. 2011;14(3):88–95. doi:10.1016/S1369-7021(11)70058-X
2. Behzadi S, Luther GA, Harris MB, et al. Nanomedicine for safe healing of bone trauma: opportunities and challenges. *Biomaterials*. 2017;146:168–182. doi:10.1016/j.biomaterials.2017.09.005
3. Besinis A, De Peralta T, Tredwin CJ, et al. Review of nanomaterials in dentistry: interactions with the oral microenvironment, clinical applications, hazards, and benefits. *ACS Nano*. 2015;9(3):2255–2289. doi:10.1021/nn505015e
4. Penkov OV, Pukha VE, Starikova SL, et al. Highly wear-resistant and biocompatible carbon nanocomposite coatings for dental implants. *Biomaterials*. 2016;102:130–136. doi:10.1016/j.biomaterials.2016.06.029
5. de Jonge LT, Leeuwenburgh SCG, van Den Beucken JJJP, et al. The osteogenic effect of electrosprayed nanoscale collagen/calcium phosphate coatings on titanium. *Biomaterials*. 2010;31(9):2461–2469. doi:10.1016/j.biomaterials.2009.11.114
6. Roohani-Esfahani S-I, Nouri-Khorasani S, Lu Z, et al. The influence hydroxyapatite nanoparticle shape and size on the properties of biphasic calcium phosphate scaffolds coated with hydroxyapatite–PCL composites. *Biomaterials*. 2010;31(21):5498–5509. doi:10.1016/j.biomaterials.2010.03.058
7. Balani K, Anderson R, Laha T, et al. Plasma-sprayed carbon nanotube reinforced hydroxyapatite coatings and their interaction with human osteoblasts in vitro. *Biomaterials*. 2007;28(4):618–624. doi:10.1016/j.biomaterials.2006.09.013
8. Descamps S, Awitor KO, Raspal V, et al. Mechanical properties of nanotextured titanium orthopedic screws for clinical applications. *J Med Device*. 2013;7(2):0210051–0210055. doi:10.1115/1.4023705
9. Brammer KS, Frandsen CJ, Jin S. TiO2 nanotubes for bone regeneration. *Trends Biotechnol*. 2012;30(6):315–322. doi:10.1016/j.tibtech.2012.02.005
10. Camps-Font O, Figueiredo R, Valmaseda-Castellon E, et al. Postoperative infections after dental implant placement: prevalence, clinical features, and treatment. *Implant Dent.* 2015;24(6):913–919. (Electronic).
11. Chen X, Leng J, Rakesh KP, et al. Synthesis and molecular docking studies of xanthone attached amino acids as potential antimicrobial and anti-inflammatory agents. *Medchemcomm*. 2017;8(8):1706–1719. doi:10.1039/c7md00209b
12. Mohammed YHE, Manukumar HM, Rakesh KP, et al. Vision for medicine: Staphylococcus aureus biofilm war and unlocking key's for anti-biofilm drug development. *Microb Pathog*. 2018;123:339–347. doi:10.1016/j.micpath.2018.07.002
13. Zha GF, Wang SM, Rakesh KP, et al. Discovery of novel arylethenesulfonyl fluorides as potential candidates against methicillin-resistant of Staphylococcus aureus (MRSA) for overcoming multidrug resistance of bacterial infections. *Eur J Med Chem*. 2019;162:364–377. doi:10.1016/j.ejmech.2018.11.012
14. Rodríguez-Cano A, Pacha-Olivenza M-Á, Babiano R, et al. Non-covalent derivatization of aminosilanized titanium alloy implants. *Surf CoatTechnol*. 2014;245:66–73. doi:10.1016/j.surfcoat.2014.02.041
15. Yang Y, Ao H-Y, Yang S-B, et al. In vivo evaluation of the anti-infection potential of gentamicin-loaded nanotubes on titania implants. *Int J Nanomedicine*. 2016;11:2223–2234. doi:10.2147/IJN.S102752
16. Zhang H, Sun Y, Tian A, et al. Improved antibacterial activity and biocompatibility on vancomycin-loaded TiO(2) nanotubes: in vivo and in vitro studies. *Int J Nanomedicine*. 2013;8:4379–4389. doi:10.2147/IJN.S53221
17. Nie B, Long T, Ao H, et al. Covalent immobilization of enoxacin onto titanium implant surfaces for inhibiting multiple bacterial species infection and in vivo methicillin-resistant staphylococcus aureus infection prophylaxis. *Antimicrob Agents Chemother*. 2017;61:1098–6596. (Electronic). doi:10.1128/AAC.01766-16
18. Moriarty TF, Kuehl R, Coenye T, et al. Orthopaedic device-related infection: current and future interventions for improved prevention and treatment. *EFORT Open Rev*. 2016;1(4):89–99. doi:10.1302/2058-5241.1.000037
19. Besinis A, De Peralta T, Handy RD. The antibacterial effects of silver, titanium dioxide and silica dioxide nanoparticles compared to the dental disinfectant chlorhexidine on *Streptococcus mutans* using a suite of bioassays. *Nanotoxicology*. 2014;8(1):1–16. doi:10.3109/17435390.2012.742935
20. Manukumar HM, Chandrasekhar B, Rakesh KP, et al. Novel T-C@AgNPs mediated biocidal mechanism against biofilm associated methicillin-resistant Staphylococcus aureus (Bap-MRSA) 090, cytotoxicity and its molecular docking studies. *Medchemcomm*. 2017;8(12):2181–2194. doi:10.1039/c7md00486a
21. Zhang X, Manukumar HM, Rakesh KP, et al. Role of BP*C@AgNPs in Bap-dependent multicellular behavior of clinically important methicillin-resistant Staphylococcus aureus (MRSA) biofilm adherence: a key virulence study. *Microb Pathog*. 2018;123:275–284. doi:10.1016/j.micpath.2018.07.025
22. Besinis A, Hadi SD, Le HR, et al. Antibacterial activity and biofilm inhibition by surface modified titanium alloy medical implants following application of silver, titanium dioxide and hydroxyapatite nanocoatings. *Nanotoxicology*. 2017;11(3):327–338. doi:10.1080/17435390.2017.1299890
23. Varaprasad K, Raghavendra GM, Jayaramudu T, et al. Nano zinc oxide–sodium alginate antibacterial cellulose fibres. *Carbohydr Polym*. 2016;135:349–355. doi:10.1016/j.carbpol.2015.08.078
24. Soren S, Kumar S, Mishra S, et al. Evaluation of antibacterial and antioxidant potential of the zinc oxide nanoparticles synthesized by aqueous and polyol method. *Microb Pathog*. 2018;119:145–151. doi:10.1016/j.micpath.2018.03.048
25. Happy A, Soumya M, Venkat Kumar S, et al. Mechanistic study on antibacterial action of zinc oxide nanoparticles synthesized using green route. *Chem Biol Interact*. 2018;286:60–70. doi:10.1016/j.cbi.2018.03.008
26. Talebian N, Amininezhad SM, Doudi M. Controllable synthesis of ZnO nanoparticles and their morphology-dependent antibacterial and optical properties. *J Photochem Photobiol*. 2013;120:66–73. doi:10.1016/j.jphotobiol.2013.01.004
27. Król A, Pomastowski P, Rafińska K, et al. Zinc oxide nanoparticles: synthesis, antiseptic activity and toxicity mechanism. *Adv Colloid Interface Sci*. 2017;249:37–52. doi:10.1016/j.cis.2017.07.033
28. Cao B, Cai W, Duan G, et al. A template-free electrochemical deposition route to ZnO nanoneedle arrays and their optical and field emission properties. *Nanotechnology*. 2005;16(11):2567. doi:10.1088/0957-4484/16/11/017

29. Roguska A, Belcarz A, Pisarek M, et al. TiO2 nanotube composite layers as delivery system for ZnO and Ag nanoparticles — an unexpected overdose effect decreasing their antibacterial efficacy. *Mater Sci Eng*. 2015;51:158–166. doi:10.1016/j.msec.2015.02.046
30. Li X, Wang C, Xia N, et al. Novel ZnO-TiO2 nanocomposite arrays on Ti fabric for enhanced photocatalytic application. *J Mol Struct*. 2017;1148:347–355. doi:10.1016/j.molstruc.2017.07.030
31. Ma Q-L, Ma S, Huang YM. Enhanced photovoltaic performance of dye sensitized solar cell with ZnO nanohoneycombs decorated TiO2 photoanode. *Mater Lett*. 2018;218:237–240. doi:10.1016/j.matlet.2018.02.028
32. Chansri P, Sung Y-M. Investigations of electrochemical luminescence characteristics of ZnO/TiO2 nanotubes electrode and silica-based gel type solvents. *Surf CoatTechnol*. 2016;307:1139–1143. doi:10.1016/j.surfcoat.2016.11.009
33. Lin Y-J, Chang G-M, Chang H-C, et al. Responsivity to solar irradiation and the response time of photodetectors that use ZnO nanoparticles with and without thermal annealing in pure oxygen ambient. *Optik*. 2018;155:157–162. doi:10.1016/j.ijleo.2017.11.012
34. Chia SL, Leong DT. Reducing ZnO nanoparticles toxicity through silica coating. *Heliyon*. 2016;2(10):e00177. doi:10.1016/j.heliyon.2016.e00177
35. Foroutan T, Mousavi S. The effects of zinc oxide nanoparticles on differentiation of human mesenchymal stem cells to osteoblast. *Nanomed J*. 2014;1(5):308–314.
36. Ramires PA, Romito A, Cosentino F, et al. The influence of titania/hydroxyapatite composite coatings on in vitro osteoblasts behaviour. *Biomaterials*. 2001;22(12):1467–1474.
37. Ha S-W, Jang HL, Nam KT, et al. Nano-hydroxyapatite modulates osteoblast lineage commitment by stimulation of DNA methylation and regulation of gene expression. *Biomaterials*. 2015;65:32–42. doi:10.1016/j.biomaterials.2015.06.039
38. Swank K, Dragoo JL. Postarthroscopic infection in the knee following medical or dental procedures. *Case Rep Orthop*. 2013;2013:974017.
39. Danookdharree U, Le HR, Tredwin C. The effect of initial etching sites on the morphology of TiO2 nanotubes on Ti-6Al-4V alloy. *J Electrochem Soc*. 2015;162(10):E213–E222. doi:10.1149/2.0011511jes
40. Liu J, Hosseinpour PM, Luo S, et al. TiO2 nanotube arrays for photocatalysis: effects of crystallinity, local order, and electronic structure. *J Vac Sci Technol A*. 2015;33(2). doi:10.1116/1.4902350
41. Parcharoen Y, Kajitvichyanukul P, Sirivisoot S, et al. Hydroxyapatite electrodeposition on anodized titanium nanotubes for orthopedic applications. *Appl Surf Sci*. 2014;311:54–61. doi:10.1016/j.apsusc.2014.04.207
42. Liu W, Su P, Chen S, et al. Synthesis of TiO2 nanotubes with ZnO nanoparticles to achieve antibacterial properties and stem cell compatibility. *Nanoscale*. 2014;6(15):9050–9062. doi:10.1039/c4nr01531b
43. Kokubo T. Apatite formation on surfaces of ceramics, metals and polymers in body environment. *Acta Mater*. 1997;46(7):8.
44. Besinis A, De Peralta T, Handy RD. Inhibition of biofilm formation and antibacterial properties of a silver nano-coating on human dentine. *Nanotoxicology*. 2014;8(7):745–754. doi:10.3109/17435390.2013.825343
45. Tsikandylakis G, Berlin O, Branemark R. Implant survival, adverse events, and bone remodeling of osseointegrated percutaneous implants for transhumeral amputees. *Clin Orthop Relat Res*. 2014;472(10):2947–2956. doi:10.1007/s11999-014-3695-6
46. Zhao L, Chu PK, Zhang Y, et al. Antibacterial coatings on titanium implants. *J Biomed Mater Res Part B*. 2009;91B(1):470–480. doi:10.1002/jbm.b.31463
47. Li L-H, Kim H-W, Lee S-H, et al. Biocompatibility of titanium implants modified by microarc oxidation and hydroxyapatite coating. *J Biomed Mater Res Part A*. 2005;73A(1):48–54. doi:10.1002/jbm.a.30244
48. Anders CB, Eixenberger JE, Franco NA, et al. ZnO nanoparticle preparation route influences surface reactivity, dissolution and cytotoxicity. *Environ Sci*. 2018;5(2):572–588. doi:10.1039/C7EN00888K
49. Liu X, Tian A, You J, et al. Antibacterial abilities and biocompatibilities of Ti-Ag alloys with nanotubular coatings. *Int J Nanomedicine*. 2016;11:5743–5755. doi:10.2147/IJN.S113674
50. Aarestrup FM, Hasman H. Susceptibility of different bacterial species isolated from food animals to copper sulphate, zinc chloride and antimicrobial substances used for disinfection. *Vet Microbiol*. 2004;100(1):83–89. doi:10.1016/j.vetmic.2004.01.013
51. Babich H, Stotzky G. Toxicity of zinc to fungi, bacteria, and coliphages: influence of chloride ions. *Appl Environ Microbiol*. 1978;36(6):906–914.
52. Baek YW, An YJ. Microbial toxicity of metal oxide nanoparticles (CuO, NiO, ZnO, and Sb2O3) to Escherichia coli, Bacillus subtilis, and Streptococcus aureus. *Sci Total Environ*. 2011;409:1603–1608. doi:10.1016/j.scitotenv.2011.01.014
53. Reidy B, Haase A, Luch A, et al. Mechanisms of silver nanoparticle release, transformation and toxicity: a critical review of current knowledge and recommendations for future studies and applications. *Materials*. 2013;6(6):2295. doi:10.3390/ma6062295
54. Saxena V, Hasan A, Pandey LM. Effect of Zn/ZnO integration with hydroxyapatite: a review. *Mater Technol*. 2018;33(2):79–92. doi:10.1080/10667857.2017.1377972
55. Plette ACC, Benedetti MF, van Riemsdijk WH. Competitive binding of protons, calcium, cadmium, and zinc to isolated cell walls of a gram-positive soil bacterium. *Environ Sci Technol*. 1996;30(6):1902–1910. doi:10.1021/es950568l
56. Gunputh UF, Le H, Handy RD, et al. Anodised TiO2 nanotubes as a scaffold for antibacterial silver nanoparticles on titanium implants. *Mater Sci Eng*. 2018;91:638–644. doi:10.1016/j.msec.2018.05.074

Supplementary material

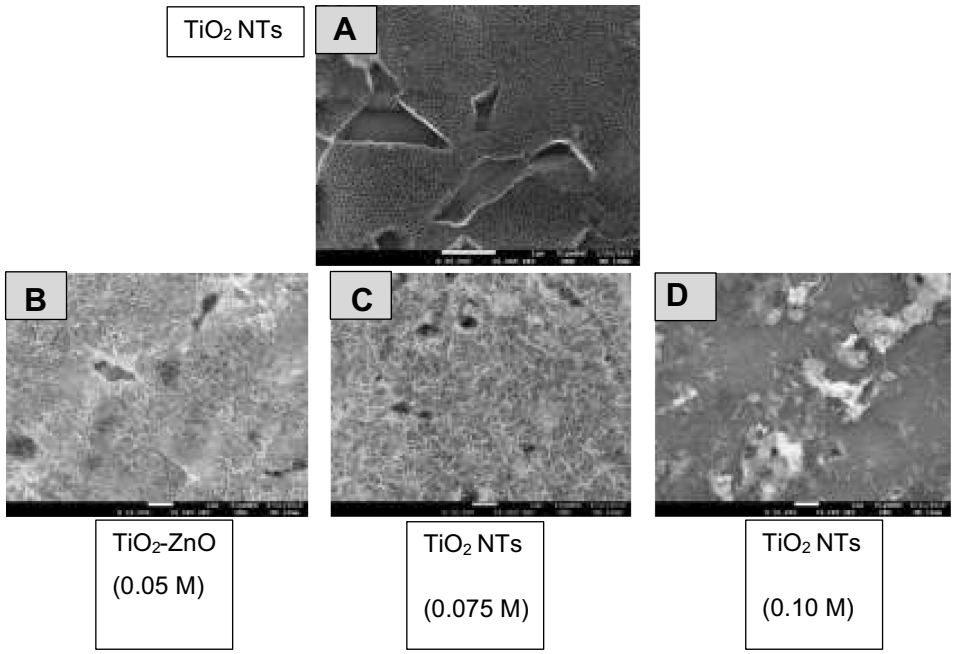

Figure S1 The resulting TiO_2 NTs (**A**), nZnO coatings on TiO_2 NTs synthesized in the presence of 0.05 M (**B**), 0.075 M (**C**), and 0.10 M (**D**) zinc nitrate as viewed under the high-resolution scanning electron microscopy.